AD-A194 134 WAVE STRUCTURES IN THERMOSPHERIC DENSITY FROM SATELLITE ELECTROSTATIC TRIAXIAL ACCELEROMETER MEASUREMENTS(U) AIR FORCE GEOPHYSICS LAB HANSCOM AFB MA 04 JUN 87 AFGL-TR-87-0189 1/1

UNCLASSIFIED F/G 4/1 NL

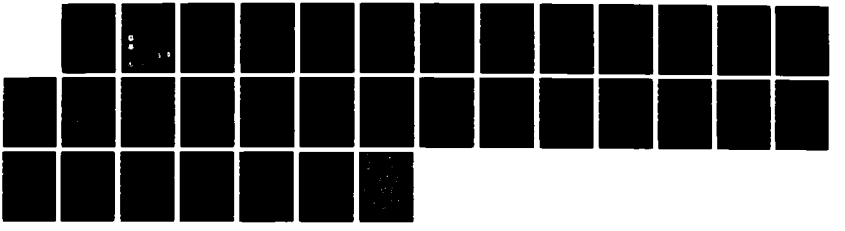

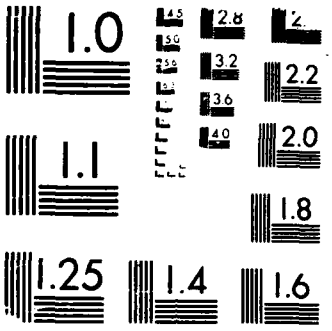

MICROCOPY RESOLUTION TEST CHART

(ANSI and ISO) STANDARDS 1963-A

AFGL-TR- 87-0189
ENVIRONMENTAL RESEARCH PAPERS, NO. 976

Wave Structures in Thermospheric Density From Satellite Electrostatic Triaxial Accelerometer Measurements

J.M. FORBES
F.A. MARCOS
P.F. FOUGERE

4 June 1987

IONOSPHERIC PHYSICS DIVISION PROJECT 6670
AIR FORCE GEOPHYSICS LABORATORY
HANSCOM AFB, MA 01731

This report has been reviewed by the ESD Public Affairs Office (PA) and is releasable to the National Technical Information Service (NTIS).

"This technical report has been reviewed and is approved for publication"

FOR THE COMMANDER

HERBERT C. CARLSON
Branch Chief

ROBERT A. SKRIVANEK
Division Director

Qualified requestors may obtain additional copies from the Defense Technical Information Center. All others should apply to the National Technical Information Service.

If your address has changed, or if you wish to be removed from the mailing list, or if the addressee is no longer employed by your organization, please notify AFGL/DAA, Hanscom AFB, MA 01731. This will assist us in maintaining a current mailing list.

Do not return copies of this report unless contractual obligations or notices on a specific document requires that it be returned.

AFGL-TR-87-0189
ENVIRONMENTAL RESEARCH PAPERS, NO. 976

Wave Structures in Thermospheric Density From Satellite Electrostatic Triaxial Accelerometer Measurements

J. M. Forbes
F. A. Marcos
P. F. Fougere

4 June 1987

E R R A T A

PUBLICATION DATE (ON PAGE 1 - FOLLOWING TEXT) SHOULD READ AS FOLLOWS, AND NOT AS SHOWN IN REPORT:

(Received for publication 2 June 1987)

AIR FORCE GEOPHYSICS LABORATORY
AIR FORCE SYSTEMS COMMAND
UNITED STATES AIR FORCE
HANSCOM AIR FORCE BASE, MASSACHUSETTS 01731

Unclassified
SECURITY CLASSIFICATION OF THIS PAGE

ADA194134

REPORT DOCUMENTATION PAGE

Form Approved OMB No. 0704-0188

1a. REPORT SECURITY CLASSIFICATION: Unclassified	1b. RESTRICTIVE MARKINGS
2a. SECURITY CLASSIFICATION AUTHORITY	3. DISTRIBUTION/AVAILABILITY OF REPORT: Approved for public release; distribution unlimited
2b. DECLASSIFICATION/DOWNGRADING SCHEDULE	
4. PERFORMING ORGANIZATION REPORT NUMBER(S): AFGL-TR-87-0189 ERP, No. 976	5. MONITORING ORGANIZATION REPORT NUMBER(S)
6a. NAME OF PERFORMING ORGANIZATION: Air Force Geophysics Laboratory; 6b. OFFICE SYMBOL (If applicable): LIS	7a. NAME OF MONITORING ORGANIZATION
6c. ADDRESS (City, State, and ZIP Code): Hanscom AFB Massachusetts 01731	7b. ADDRESS (City, State, and ZIP Code)
8a. NAME OF FUNDING/SPONSORING ORGANIZATION; 8b. OFFICE SYMBOL (If applicable)	9. PROCUREMENT INSTRUMENT IDENTIFICATION NUMBER
8c. ADDRESS (City, State, and ZIP Code)	10. SOURCE OF FUNDING NUMBERS: PROGRAM ELEMENT NO. 62101F; PROJECT NO. 6670; TASK NO. 18; WORK UNIT ACCESSION NO. 05

11. TITLE (Include Security Classification)
Wave Structures in Thermospheric Density from Satellite Electrostatic Triaxial Accelerometer Measurements

12. PERSONAL AUTHOR(S)
Jeffrey M. Forbes*, Frank A. Marcos, and Paul F. Fougere

13a. TYPE OF REPORT	13b. TIME COVERED	14. DATE OF REPORT (Year, Month, Day)	15. PAGE COUNT
Scientific. Final	FROM _____ TO _____	1987 June 4	30

16. SUPPLEMENTARY NOTATION
*Dept. of Electrical, Computer and Systems Engineering, Boston University, Boston, Massachusetts 02215

17. COSATI CODES		
FIELD	GROUP	SUB-GROUP
04	01	
22	03	

18. SUBJECT TERMS (Continue on reverse if necessary and identify by block number)
Atmospheric density, Satellite accelerometers, Atmospheric wave structures, Maximum entropy method

19. ABSTRACT (Continue on reverse if necessary and identify by block number)

Density data from the Satellite Electrostatic Triaxial Accelerometer (SETA) experiment were spectrally analyzed by the Maximum Entropy Method (MEM). The purpose is to make available a technique by which the occurrence of wavelike structures in thermospheric densities can be quantitatively analyzed and correlated with various geophysical conditions, including the deposition of energy at high latitudes during geomagnetically disturbed conditions. Spectra were computed for typical magnetically quiet and active days during July 1983, and the relative occurrence of spectral peaks in wavelength ranges of large-scale (hundreds to thousands of kilometers) and medium-scale (tens to hundreds of kilometers) traveling ionospheric disturbances is examined as a function of local time and latitude.

20. DISTRIBUTION/AVAILABILITY OF ABSTRACT	21. ABSTRACT SECURITY CLASSIFICATION
☒ UNCLASSIFIED/UNLIMITED ☐ SAME AS RPT ☐ DTIC USERS	Unclassified
22a. NAME OF RESPONSIBLE INDIVIDUAL: Frank A. Marcos	22b. TELEPHONE (Include Area Code): (617) 377-3037; 22c. OFFICE SYMBOL: LIS

DD Form 1473, JUN 86 *Previous editions are obsolete.*

Contents

Illustrations

Illustrations

Tables

Wave Structures in Thermospheric Density from Satellite Electrostatic Triaxial Accelerometer Measurements

1. INTRODUCTION

The frequent occurrence of wavelike perturbations in thermospheric and ionospheric constituent densities, winds, and temperatures is now universally accepted, although the origin and propagation characteristics of these oscillations are poorly understood and still under investigation.[1,2] Historically, the first comprehensive studies[3,4] involved the analysis of ionospheric data, and the wave motions were referred to as 'travelling ionospheric disturbances' (TIDs) although it was known that fluctuations in ionospheric parameters were actually driven by collisions with the oscillating neutral gas. Georges[3] categorized these waves

(Received for publication for publication 2 June 1987)

1. Mayr, H.G., Harris, I., Varosi, F., and Herrero, F.A. (1984) Global excitation of wave phenomena in a dissipative multiconstituent medium. 1. Transfer function of the Earth's thermosphere, J. Geophys. Res., 89:10929.

2. Mayr, H.G., Harris, I., Varosi, F., and Herrero, F.A. (1984) Global excitation of wave phenomena in a dissipative multiconstituent medium. 2. Impulsive perturbations in the Earth's thermosphere, J. Geophys. Res., 89:10961.

3. Georges, T.M. (1968) HF Doppler studies of travelling ionospheric disturbances, J. Atmos. Terr. Phys., 30:735.

4. Testud, J. (1970) Gravity waves generated during magnetic substorms, J. Atmos. Terr. Phys., 32:1793.

according to their horizontal wavelengths as being either large-scale (1000 to 4000 km) or medium-scale (100 to 500 km). The large-scale waves are also characterized by periods of order 1 to 3 hours and propagation velocities of order 0.5 to 1.0 km/sec, and are thought to be primarily excited during substorms by impulsively enhanced particle precipitation heating, Lorentz forces, and joule dissipation at high latitudes.[5,6,7] The large-scale waves can propagate long distances from the source and are detectable at low latitudes.[8,9] The medium-scale waves propagate slowly (100 to 250 m/sec) and have periods in the range of 15 to 60 minutes. Their origin is less certain, but they have been tenuously connected with meteorological sources in the troposphere.[10,11,12,13] Medium-scale waves propagating horizontally away from an auroral source do not travel long distances; however, it is thought that medium-scale waves partially reflected at the base of the thermosphere[14] or totally reflected at the surface[15] may be ducted into the thermosphere with little attenuation and travel large distances from the source.[1,2,16,17]

---

5. Thome, G. (1968) Long-period waves generated in the polar ionosphere during the onset of magnetic storms, J. Geophys. Res., 73:6319.
6. Davis, M.J., and da Rosa, A.V. (1969) Traveling ionospheric disturbances originating in the auroral oval during polar substorms, J. Geophys. Res., 74:5721.
7. Testud, J.P., Amayenc, P., and Blanc, M. (1975) Middle and low latitude effects of auroral disturbances from incoherent scatter, J. Atmos. Terr. Phys., 37:989.
8. Harper, R.M. (1972) Observation of a large nighttime gravity wave at Arecibo, J. Geophys. Res., 77:1311.
9. Herrero, F.A., and Meriwether, J.W. (1981) Equatorial nighttime F-region events: A survey of 6300 Å airglow intensity maps at Arecibo, J. Atmos. Terr. Phys., 43:859.
10. Beer, T. (1974) Atmospheric Waves. John Wiley, New York.
11. Larsen, M.F., Swartz, W.E., and Woodman, R.F. (1982) Gravity wave generation by thunderstorms observed with a vertically-pointing 430 MHz radar, Geophys. Res. Lett., 9:571.
12. Mastrantonio, G.F., Einaudi, F., Fua, D., and Lalas, D.P. (1976) Generation of gravity waves by jet streams in the atmosphere, J. Atmos. Sci., 33:1730.
13. Bertin, F.J., Testud, J., Kersley, L., and Rees, P.R. (1978) The meteorological jet stream as a source of medium scale gravity waves in the thermosphere: An experimental study, J. Atmos. Terr. Phys., 40:1161.
14. Richmond, A.D. (1978) The nature of gravity wave ducting in the thermosphere, J. Geophys. Res., 83:1385.
15. Francis, S.H. (1974) A theory of medium-scale traveling ionospheric disturbances, J. Geophys. Res., 79:5245.
16. Hines, C.O. (1960) Internal atmospheric gravity waves at ionospheric heights, Can. J. Phys., 38:1441.
17. Friedman, J.P. (1966) Propagation of internal gravity waves in a thermally stratified atmosphere, J. Geophys. Res., 71:1033.

The experimental view based on wave analyses[18] of neutral and ion density and temperature measurements from the AE-C satellite is that a quasi-stationary, quasi-persistent wave structure (scales of order 400 to 4000 km) that may slowly dissipate and be regenerated by auroral-region sources exists over global distances in the thermosphere.

The above theoretical studies and experimental results suggest a need for wave analyses of satellite measurements that focus on the latitudinal and magnetic activity dependences of the wave characteristics. An existing data base[19] consisting of low-altitude (160 to 220 km) densities measured from a series of Air Force satellite accelerometer experiments is ideally suited for this purpose, as there exist many consecutive orbits of data ranging from high to low latitudes in a high-inclination orbit (~ 80 to 85°) covering both quiet and active magnetic conditions between 1979 and 1985. Density data from the Satellite Electrostatic Triaxial Accelerometer (SETA) Experiment were spectrally analyzed by the Maximum Entropy Method (MEM). The purpose is to make available a technique by which the occurrence of wavelike structures in thermospheric densities can be quantitatively analyzed and correlated with various geophysical conditions, including the deposition of energy at high latitudes during geomagnetically disturbed conditions. Spectra were computed for typical magnetically quiet and active days during July 1983, and the relative occurrence of spectral peaks in wavelength ranges characteristic of large-scale and medium-scale TIDs is examined as a function of local time and latitude.

2. DESCRIPTION OF DATA AND PROCESSING STEPS

2.1 The SETA Experiment

The Satellite Electrostatic Triaxial Accelerometer Experiment (SETA) is based on the single-axis MESA instrument flown by the Air Force Geophysics Laboratory on eight satellites since 1968 including Atmosphere Explorers C, D, and E. The MESA utilizes a proof mass in the shape of a flanged, hollow cylinder. This proof mass is suspended electrostatically along its radial axes and is force-rebalanced electrostatically along its longitudinal or sensitive axis. A complete description

18. Gross, S.H., Reber, C.A., and Huang, F.T. (1984) Large-scale waves in the thermosphere observed by the AE-C satellite, IEEE Trans. on Geos. and Remote Sens., GE-22:340.

19. Marcos, F.A. (1987) Requirements for improved thermospheric models, J. Astronaut. Sci., in press.

of the MESA instrument flown on the three Atmosphere Explorer satellites is given by Champion and Marcos.[20] To develop a triaxial-sensing capability, the suspension system was modified by instrumenting both radial axes with precision constrainment loops. A complete description of the SETA configuration is given by Marcos and Swift.[21] Marcos and Swift[21] also describe results of an orbital flight test from which various instrument response characteristics and design improvements were obtained.

The accelerometer output contains contributions related to vehicle dynamics and instrument operating characteristics as well as those due to aerodynamic drag and winds. Centripetal acceleration and the gravity gradient effect, each of the order of 0.32 μg but oppositely directed, provide a negligible (< 0.01 μg) resultant dynamic acceleration in the along-track (Z) axis. Extraneous accelerometer outputs consist of a bias a_B and random noise a_N. With the centripetal and gravity gradient accelerations incorporated as part of the bias term and the vehicle dynamic acceleration represented by a_v the average accelerometer output over the 2.045-sec sample time a_T is then represented by

$$a_{Ti} = a_{Di} + a_{vi} + a_{Bi} + a_{Ni} \qquad (1)$$

where i = X, Y, Z, since the various acceleration sources can be different along each axis. The aerodynamic component is derived using Eq. (1) in the form

$$a_{Di} = a_{Ti} - (a_{vi} + a_{Bi} + a_{Ni}) .$$

Numerical filtering techniques[22] are used to remove frequency components of a_T due to satellite dynamics a_v and instrument noise a_N. The cutoff frequency of the low-pass filter is 0.066 Hz (see Section 2.2). Since the along-track accelerometer axis senses aerodynamic drag throughout the orbit, bias cannot be directly deduced by the accelerometer output at maximum altitude. A bias value is estimated

20. Champion, K.S.W., and Marcos, F.A. (1973) The triaxial accelerometer system on Atmosphere Explorer, Radio Sci., 8:197.

21. Marcos, F.A., and Swift, E.R. (1982) Application of the Satellite Triaxial Accelerometer Experiment to Atmospheric Density and Wind Studies, AFGL-TR-82-0091, AD A120852.

22. Noonan, J.P., Fioretti, R.W., and Hass, B. (1975) Digital Filtering Analysis Applied to the Atmosphere Explorer-C Satellite MESA Accelerometer Data, AFCRL-TR-75-0293, AD A015765.

for each orbit essentially by subtracting a drag acceleration based on a model density value[23] from the filtered accelerometer output at maximum altitude. This density typically corresponds to a drag value of 0.4 μg, whereas the drag at minimum altitude (~ 170 km) is typically of the order of 8 μg. For the cross-track and radial axes, aerodynamic accelerations are negligible at maximum altitude.

The equations used for the determination of atmospheric density and wind velocities are

$$a_{Di} = \frac{A_{ref}}{2m} C_i \rho V^2 \tag{2}$$

where

- i — axis X, Y, Z;
- a_{Di} — aerodynamic acceleration along axis i;
- A_{ref} — satellite frontal area;
- m — satellite mass;
- ρ — atmospheric density;
- V — atmospheric mass velocity relative to the satellite.

$$V = -V_G + V_A + V_W \tag{3}$$

where

- V_G — inertial satellite velocity;
- V_A — atmospheric rotation velocity (assumed equal to earth's rotation velocity);
- V_W — neutral wind velocity;
- C_i — drag coefficient for axis i: $C_i = C_i(V_X, V_Y, V_Z)$, calculated from the formulation of Sentman.[24]

---

23. Jacchia, L.G. (1971) Revised Static Models of the Thermosphere and Exosphere With Empirical Temperature Profiles, Spec. Rept. 332, Smithsonian Astrophys. Observatory, Cambridge, Massachusetts.

24. Sentman, L.H. (1961) Free molecular flow theory and its application to the determination of aerodynamic forces, Rept. LMSC-448514, Lockheed Missiles and Space Co., Sunnyvale, California.

In Eq. (2) only three acceleration measurements are available (a_i), while there are four unknowns (ρ, V). An iterative technique has been developed to determine density and winds. The known contributions to the Z axis velocity V_Z (that is, $-V_{GZ} + V_{AZ}$) are large compared to the uncertainty V_{WZ}; hence an initial estimate of the density is obtained by assuming $V_0 = -V_G + V_A$ and calculating

$$\rho_0 = a_{DZ} \left[\left(\frac{1}{2} \frac{A_{ref}}{2m} \right) V_0^2 C_Z(V_0) \right]^{-1} \quad (4)$$

This density estimate is used to calculate the three velocity components (V) from Eq. (2) and to obtain the wind as $V_W = V - V_0$. To refine the solution, a new $V = (V_X, V_Y, V_{0Z})$ is used in Eq. (4) to calculate a new ρ. This new ρ is then used to calculate new velocities, and so on, until convergence is achieved. The wind velocity and density estimate are accepted as final if $|V_{WZ}| < 0.002 |V_Z|$.

The errors in the calculated values of density are attributed to accelerometer bias, attitude uncertainties, drag coefficient estimates, noise within the desired signal frequency spectrum, and the inseparability of density and winds along the in-track axis. Systematic errors due to the drag coefficient are estimated to be within ±5 percent, while those due to bias vary from ±0.4 percent at 170 km to ±2 percent at 200 km. Low-frequency (<0.005 Hz) noise of amplitude 0.04 μg contributes a random error of ±0.5 percent at 170 km and ±2.5 percent at 200 km. In addition, an assumed wind uncertainty of 200 m/sec along the Z axis contributes a random error in ρ of ±5 percent. Attitude errors for all three axes are negligible.

2.2 Pre-Processing (Sampling, Filtering, and so on)

The SETA measurements were digitized at the rate of approximately one point per 2 seconds. The data used in the present analysis were taken at a rate of one point per 4 sec, corresponding to a Nyquist frequency of 0.125 Hz. A low-pass filter was applied to the data with a cutoff frequency of 1/15 Hz and unit response at 1/20 Hz. The maximum identifiable frequency in the data series therefore occurs in the range 0.05 to 0.07 Hz. Since the satellite's velocity is 7.8 km/sec, this translates to a minimum horizontal wavelength of order 100 to 150 km. Note that since the group velocities of TID's are generally less than 0.75 km/sec, the measurements reported here can be viewed as representative of the near-instantaneous horizontal wave structure within a given latitude segment. However, since the satellite orbital period is 90 min, no information can be deduced regarding the waves' frequencies or periods. When the term 'wave

frequency' is used in this report, one is actually referring to an effective frequency implied by the movement of the satellite through a fixed spatial wave structure.

The SETA experiment covers the 170 to 220 km height region between about 0° and 84° geographic latitude in a morning/evening (~1030 LT/2130 LT) orbit. Before applying the MEM (see Section 2.3), the downleg (evening) and upleg (morning) portions of the orbit are divided into the following segments:

Approximate Local Time	Latitudes
2130	10° - 35°
2130	30° - 55°
2130	55° - 80°
1030	80° - 55°
1030	55° - 30°
1030	35° - 10°

This was done to allow examination of differences in thermospheric wave structure as a function of latitude and local time, particularly during geomagnetic disturbances. The 25° latitude segments correspond to slightly less than 400 sec of data, or approximately 3000 km (or about 0.0025 Hz in frequency space). A high-pass filter was not applied to the data. The measurements were normalized and de-trended (using a linear least-squares fit) within each latitude segment before applying the MEM.

2.3 Spectral Analysis by the Maximum Entropy Method (MEM)

Since 1975, AFGL has been applying MEM to Air Force problems.[25] In each case, for each different type of data set, MEM has been compared to the "classical" methods, either Blackman-Tukey [BT] or the Cooley-Tukey periodogram method using the Discrete Fourier Transform [DFT]. In every case, MEM has been shown to be demonstrably superior to the classical methods. The superiority lies in both increased resolution and increased smoothness in the frequency domain and, for slowly varying, nearly stationary signals, increased resolution in the time domain. For slowly varying, non-stationary signals, a time window can be moved through the data set in such a way that each snapshot portrays a very nearly

25. Radoski, H.R., Fougere, P.F., and Zawalick, E.J. (1975) A comparison of power spectral estimates and applications of the maximum entropy method J. Geophys. Res., 80:619.

stationary process. Using MEM, a shorter time signal can be used than with the classical methods, and furthermore, MEM requires no external smoothing. Thus, spectral features that change with time can be more readily identified using MEM.

Figure 1 illustrates normalized densities measured on five successive orbits (Revs 478 to 482) on Day 201 of 1983, a period of quiet geomagnetic activity.

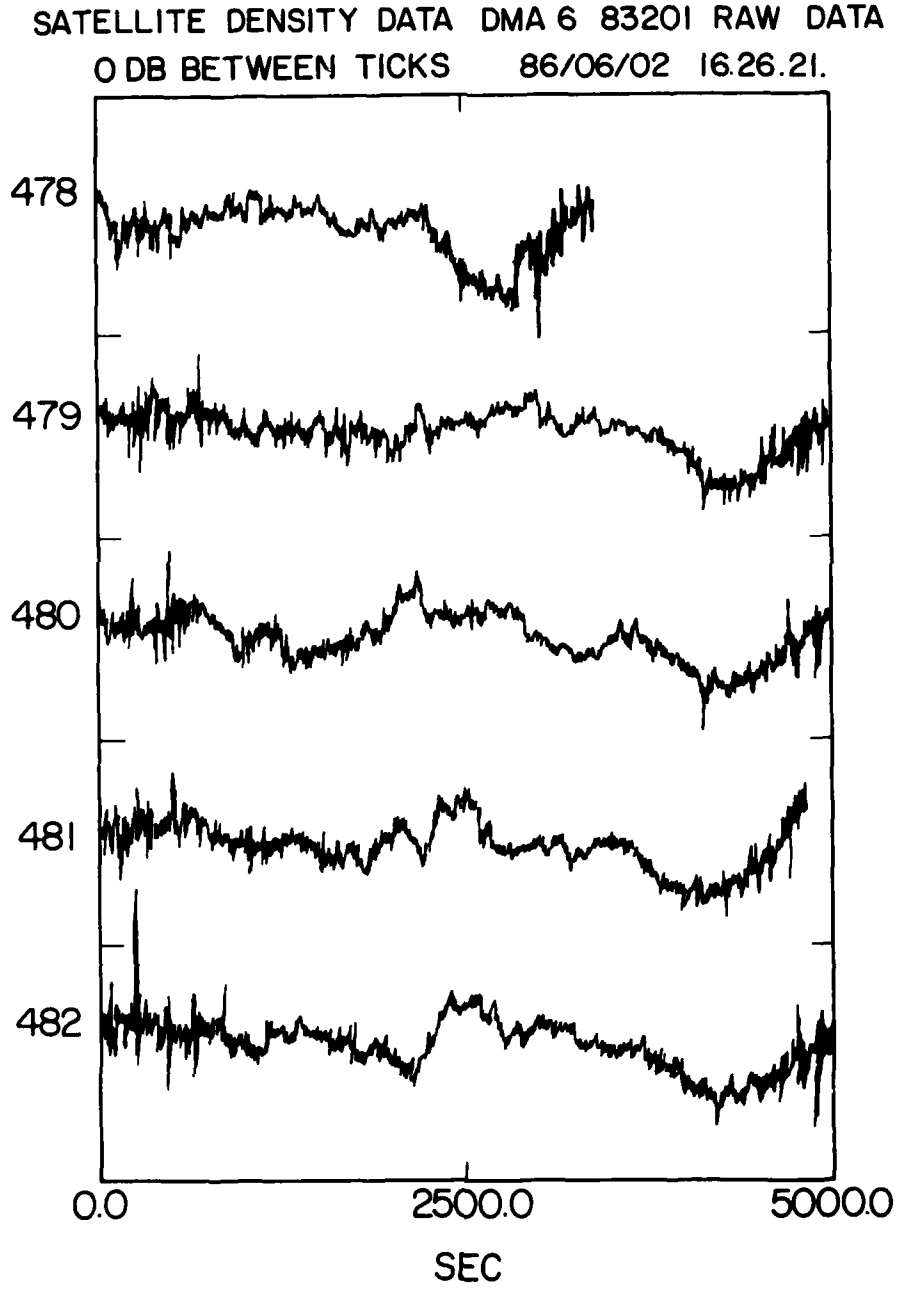

Figure 1. Normalized De-trended Densities vs Time for Revs 478-482

Figure 2 illustrates the Burg-MEM[26] spectra of order 60 between 10^{-4} and 10^{-1} Hz. The sharp falloff at about 6×10^{-2} Hz is due to the anti-aliasing filter applied before sampling.

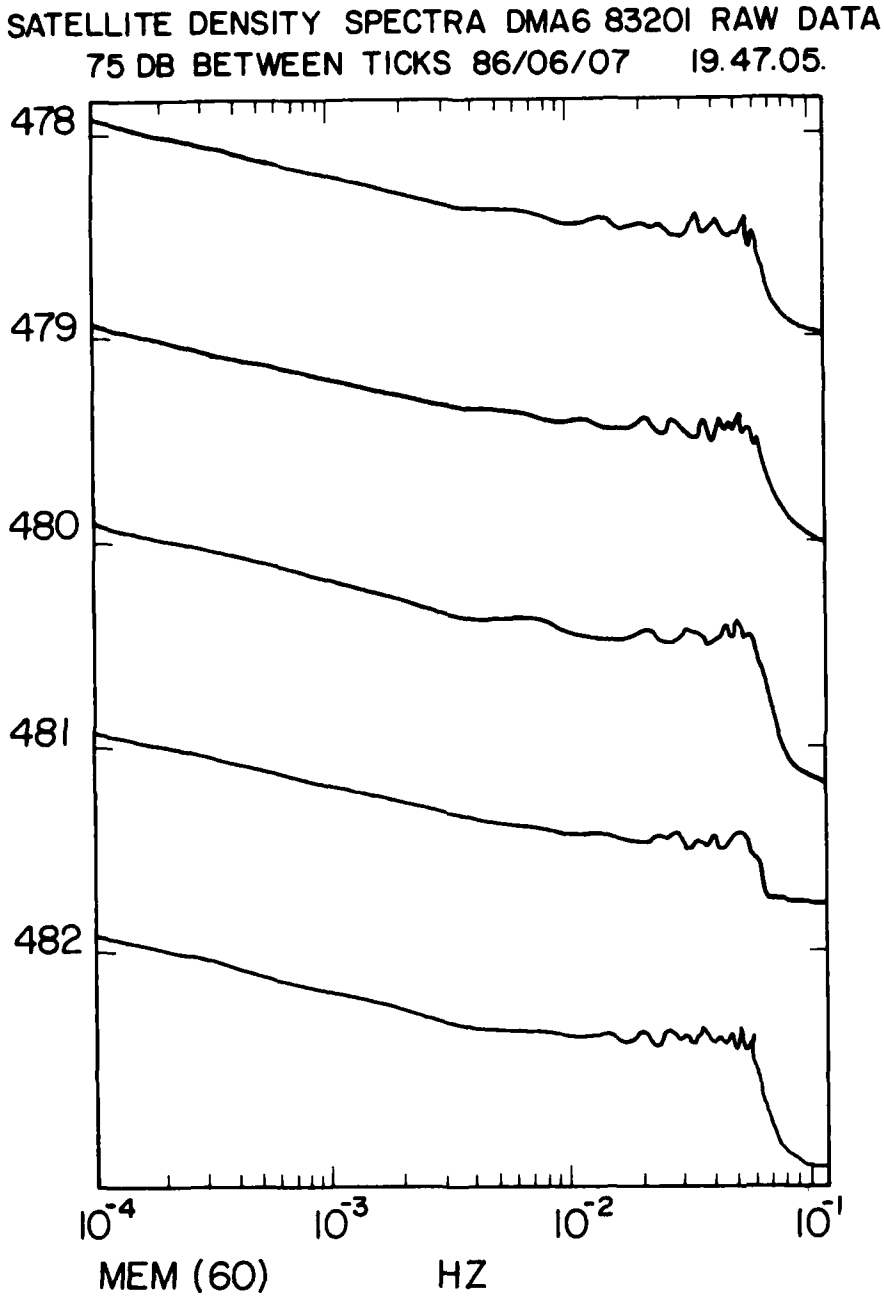

Figure 2. MEM Spectra (power spectral density vs frequency) for Normalized Densities During Revs 478-482. Tick marks represent 40-dB points for power spectral densities

26. Burg, J. P. (1981) Maximum entropy spectral analysis in Modern Spectrum Analysis, edited by D. G. Childers. IEEE Press, New York.

The order m of the MEM determines the smoothness or complexity of the spectrum. For small m the spectrum will be smooth and simple; as m increases, the resolution and complexity of the spectrum will increase. The Akaike, or final prediction error (FPE)[27] criterion for selecting the MEM order, requires that m which minimizes the FPE. However, it has been found in the satellite density data analyzed by Gross[18] that the FPE exhibits a broad and shallow minimum in all cases. For our purposes, we wish to have the simplest spectrum that identifies all the major spectral peaks characteristic of the data. The order was therefore chosen by visually examining data where certain frequencies were obviously exhibited, and by increasing m until the expected spectral peaks were adequately identified; further increasing m beyond this point did not change the dominant spectral peaks, but only added structure to the spectrum. An example of varying the order m on the spectra for a given segment of data is illustrated in Figure 3 for Rev 541 on Day 205, a period of high magnetic activity. We varied the order m from 5 to 30 in steps of 5. On the basis of these results, and for several other typical orbits which we have examined, a value of m = 25 was chosen for all the spectra to be presented here.

27. Ulryck, T.J., and Bishop, T.N. (1975) Maximum entropy spectral analysis and autoregressive decomposition, Rev. Geophys. Space Phys., 13:183.

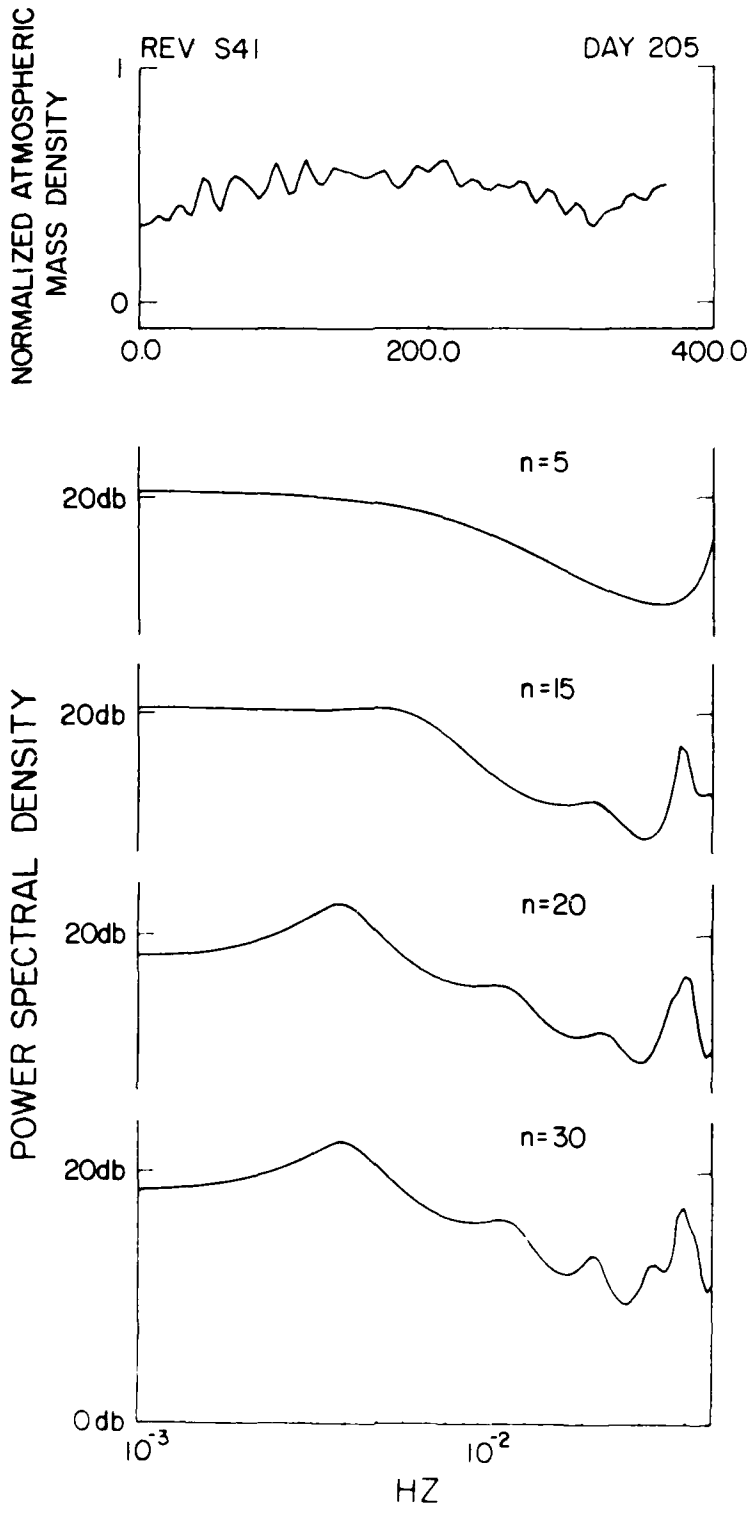

Figure 3. Densities (top panel) and Corresponding MEM Spectra of Varying Order From n = 5 to n = 30 for Rev 541

3. ANALYSIS AND INTERPRETATION OF SPECTRA

In this section, spectra computed for typical magnetically quiet and active days are presented, and their characteristics analyzed as a function of local time and latitude. Specifically, the data are taken during Days 203 and 205 of 1983, which occurred during July. The 3-hourly Kp indices are shown in the table below:

Day	Kp							
203	2+	1o	1o	1o	1-	1-	3-	5-
205	6-	5o	4o	4-	6o	4o	4o	3+

Sample normalized density data plots for Revs 511 (during the first 3 hours of Day 203) and 542 (during the first three hours of Day 205) are shown in Figures 4 through 7. The data are separated according to day (Figures 5 and 7) and night (Figures 4 and 6), and according to latitude regions (10° to 35°, 30° to 55°, and 55° to 80°). The ranges of altitudes are also shown on the plots. The Rev 542 data generally exhibit an enhanced degree of structure and waviness, presumably connected with the increase in magnetic activity. The corresponding maximum entropy spectra are shown in Figures 8 through 11. The tick marks on the spectral plots represent the 40-dB points for the power spectral density. Note that while the spectral power is considerably enhanced during the magnetically active period, and some frequency shifting of the peaks occurs, the structure of the spectrum does not appear to be appreciably enhanced as a result of the increased geomagnetic activity.

The relationship between wave spectral characteristics and geomagnetic activity, latitude, and local time requires examination of a much larger data base, however, including examination of seasonal effects as well. A comprehensive statistical and scientific analysis is beyond the scope of this report. However, we do analyze the first 14 revs (21 hours) of Days 203 and 205 of 1983, and demonstrate the type of study which can be performed with the data analysis procedure which has been set up. Specifically, we will examine Revs 509-522 of Day 203 and Revs 541-554 of Day 205 for the relative occurrence of various scale waves whose spectral density peaks exceed the 30-dB and 40-dB levels as a function of local time, latitude, and magnetic activity. Tabulations representing percent occurrence of peaks exceeding 30 dB and 40 dB are listed respectively, in Tables 1 and 2.

(Note that since occasional data gaps occurred, we have listed percent occurrence, rather than number of occurrences; however, since data gaps were fairly rare, 100 percent occurrence corresponds to no less than 12 occurrences during the day.)

Examination of Tables 1 and 2 reveals the following. First, from Table 2, we see that the most commonly occurring waves are those characterized by large horizontal scales (1250 to 2500 km). There also exists evidence of an increase in occurrence for enhanced magnetic activity conditions [with the exception of low latitudes (10° to 35°) during the morning (1030 h)]. During the quiet day the only occurrences of medium-scale waves were at high latitudes (55° to 80°) during nighttime (2030 h). This pattern persists during the magnetically active day with about twice the probability (15 to 23 percent as opposed to 8 to 15 percent). Enhanced wave activity at high latitudes during nighttime is, in fact, consistent with model simulations and data for the CDAW-6 magnetic storm period.[28,29] Further, during the magnetically disturbed day the data in Table 2 indicate an increased preference for the existence of large-scale waves as one progresses from low to high latitudes.

The percent occurrences of spectral density peaks in excess of 30 dB are listed in Table 1. Also listed at the bottom of the table are differences in percent occurrence (Day 205 minus Day 203). In almost all cases, waves of both "large" and "medium" scale occur more often than 20 percent of the time. As a result of increased magnetic activity, a general enhancement of wave activity occurs for large (1250 to 2500 km) and medium-scale (150 to 500 km) waves. We speculate that the increased occurrence of medium-scale wave activity at low and middle latitudes during magnetically disturbed periods may be attributable to ducted waves in the lower thermosphere as suggested by the theoretical calculations of Mayr et al.[1,2]

---

28. Roble, R.G., Forbes, J.M., and Marcos, F.A. (1987) Thermospheric dynamics during the March 22, 1979 magnetic storm (1) Model simulations, J. Geophys. Res., 92:6045.

29. Forbes, J.M., Roble, R.G., and Marcos, F.A. (1987) Thermospheric dynamics during the March 22, 1979 magnetic storm (2.) Comparisons of m model predictions with observations, J. Geophys. Res., 92:6069.

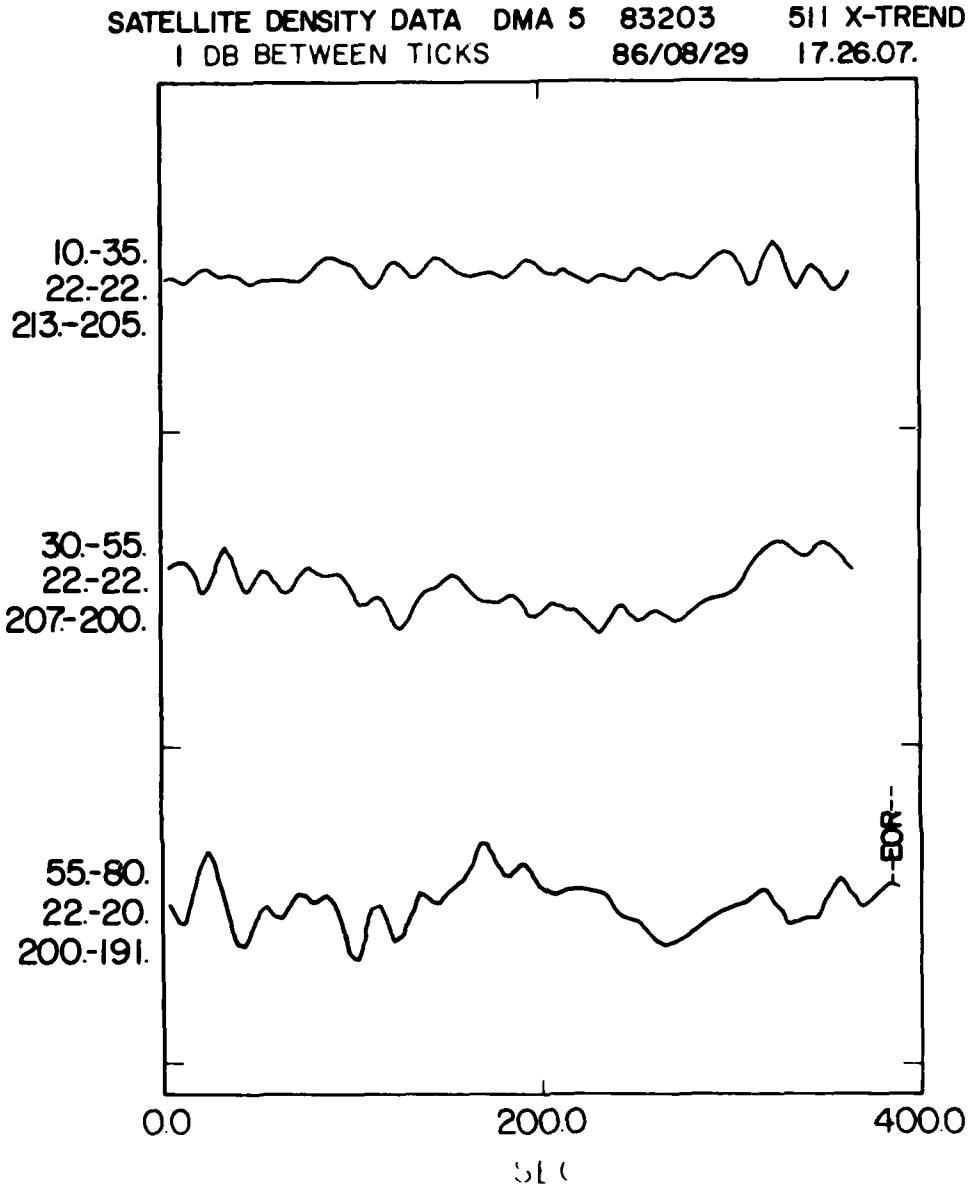

Figure 4. Normalized De-trended Densities vs Time for the Nightside (~2030 h) Portion of Rev 511. Corresponding latitudes (ranging from 10° -35° at the top, 30° -55° in the middle, and 55° -80° at the bottom) and altitudes are shown at the left

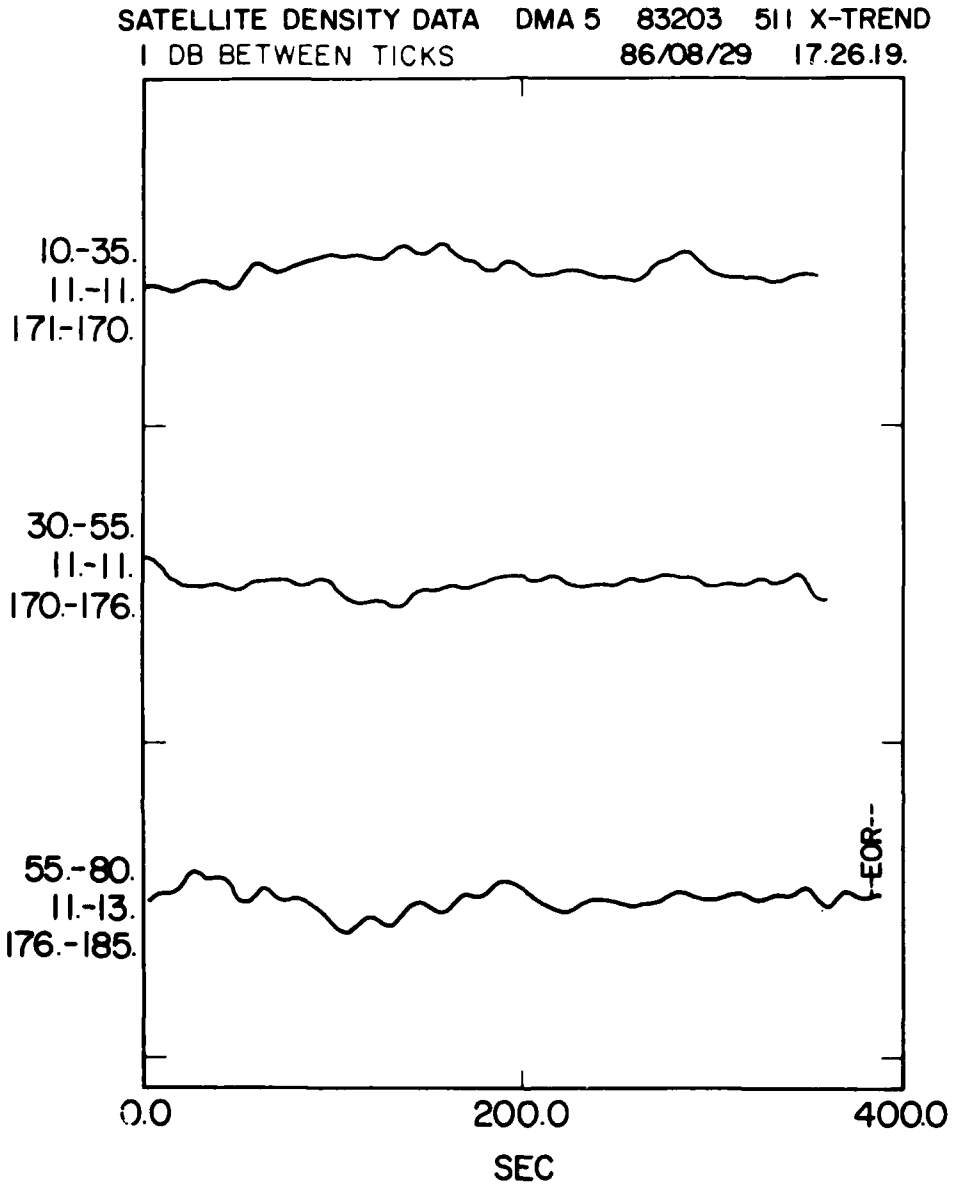

Figure 5. Normalized De-trended Densities vs Time for Daytime (~ 1030 h) Portion of Rev 511. Corresponding latitudes (ranging from 10° - 35° at the top, 30° - 55° in the middle, and 55° - 80° at the bottom) and altitudes are shown at the left

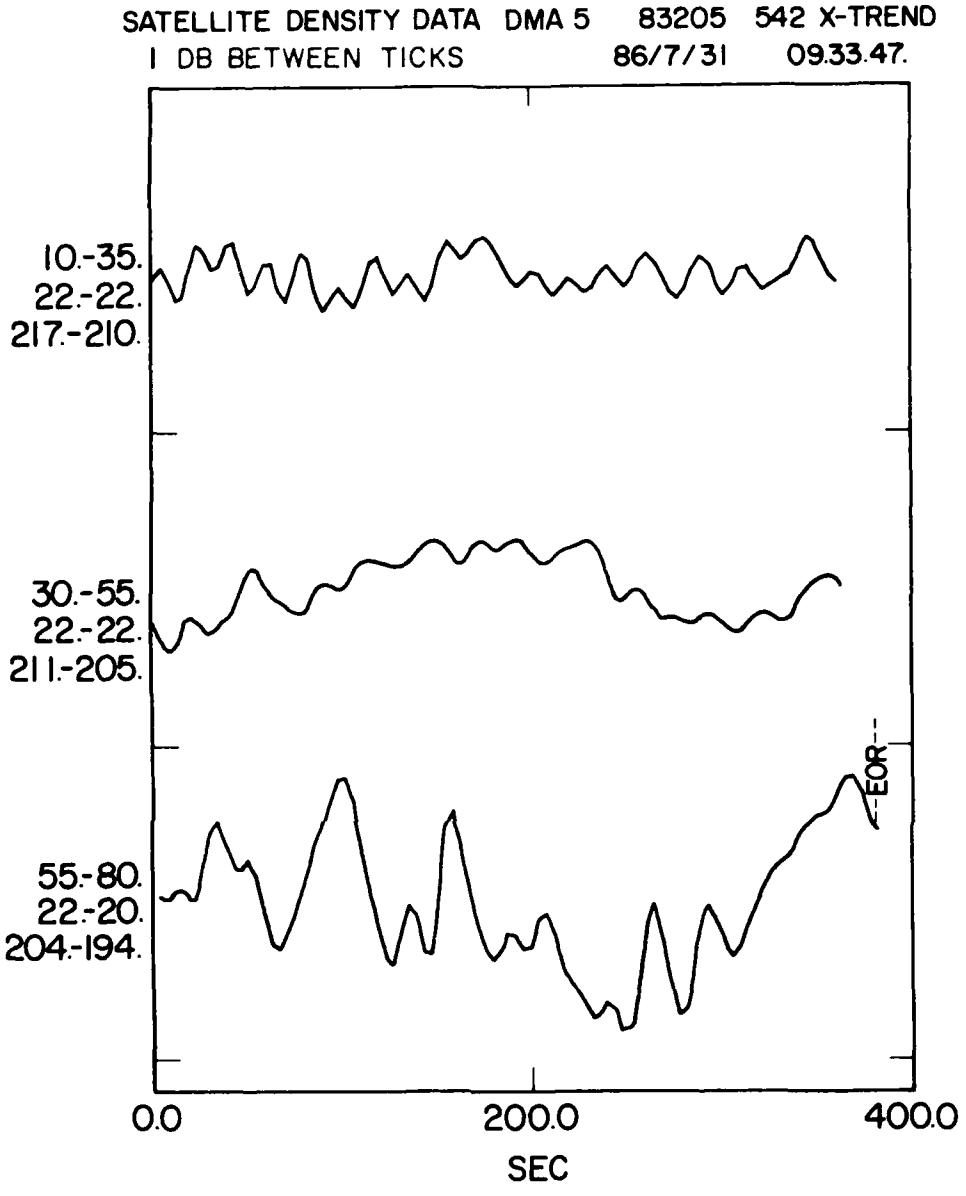

Figure 6. Normalized De-trended Densities vs Time for the Nightside (~2030 h) Portion of Rev 542. Corresponding latitudes (ranging from 10° - 35° at the top, 30° - 55° in the middle, and 55° - 80° at the bottom) and altitudes are shown at the left

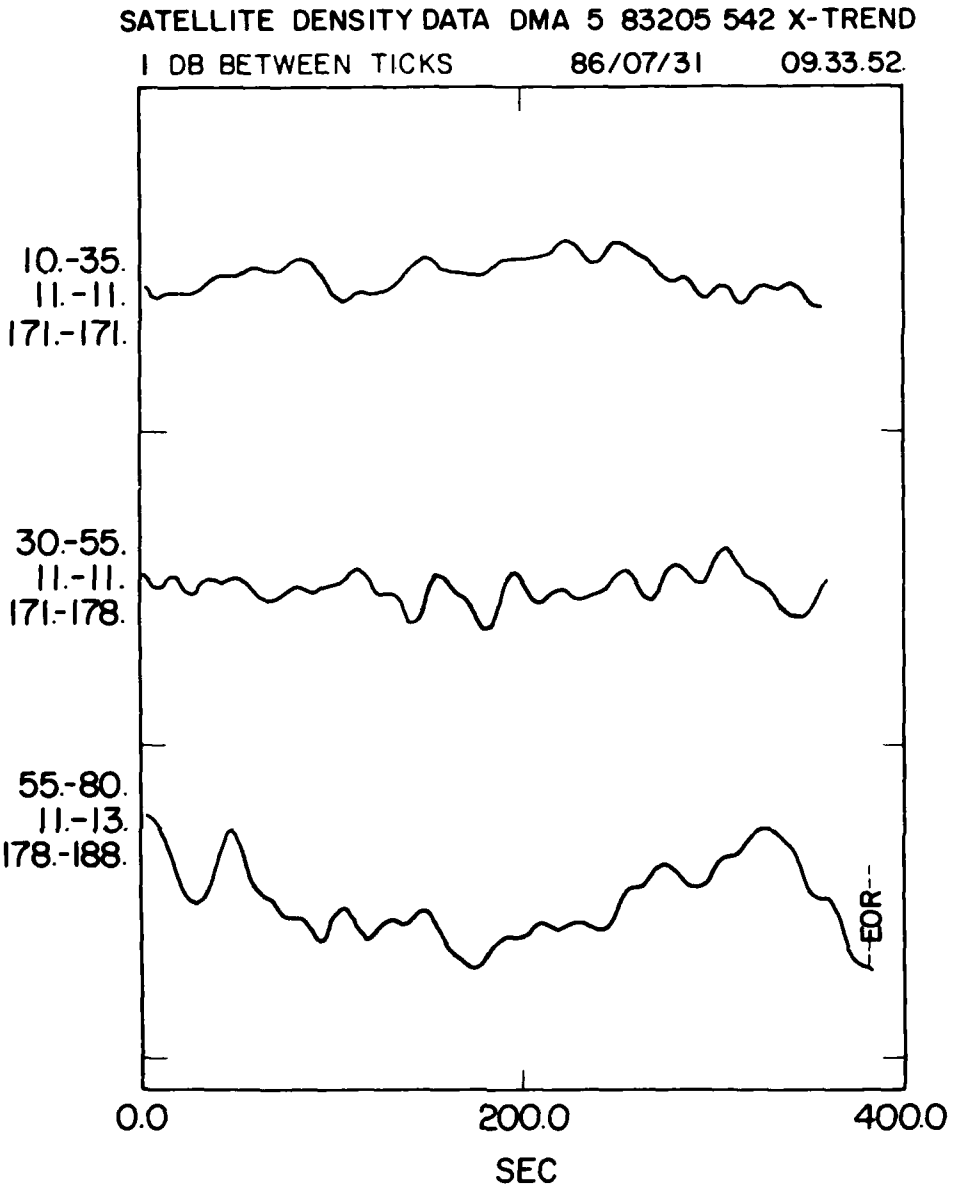

Figure 7. Normalized De-trended Densities vs Time for Daytime (~ 1030 h) Portion of Rev 542. Corresponding latitudes (ranging from 10° - 35° at the top, 30° - 55° in the middle, and 55° - 80° at the bottom) and altitudes are shown at the left

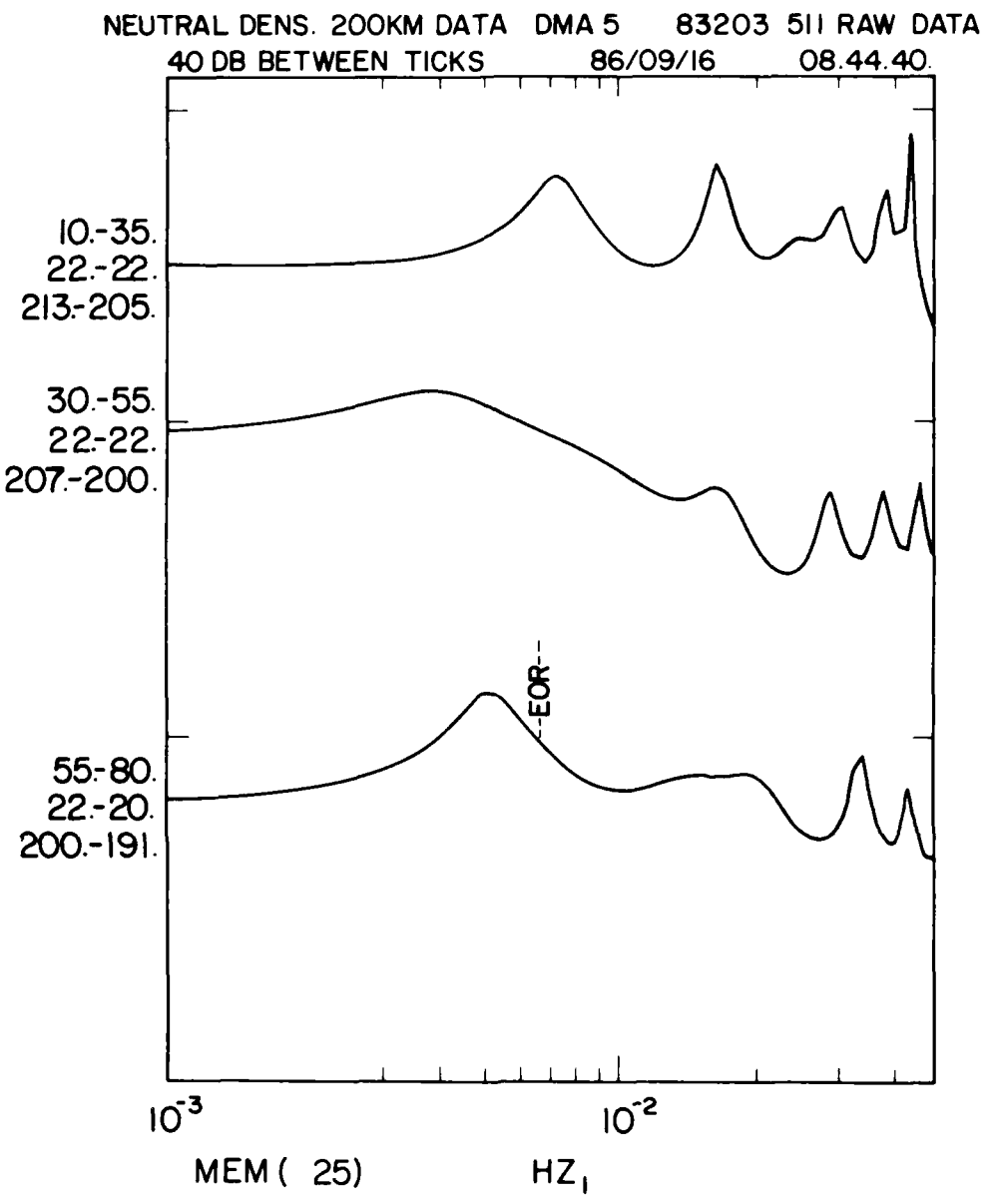

Figure 3. MEM Spectra (power spectral density vs frequency) of Order = 25 for Nightside (~ 2030 h) Portion of Rev 511. Tick marks correspond to 49-dB points for power spectral density

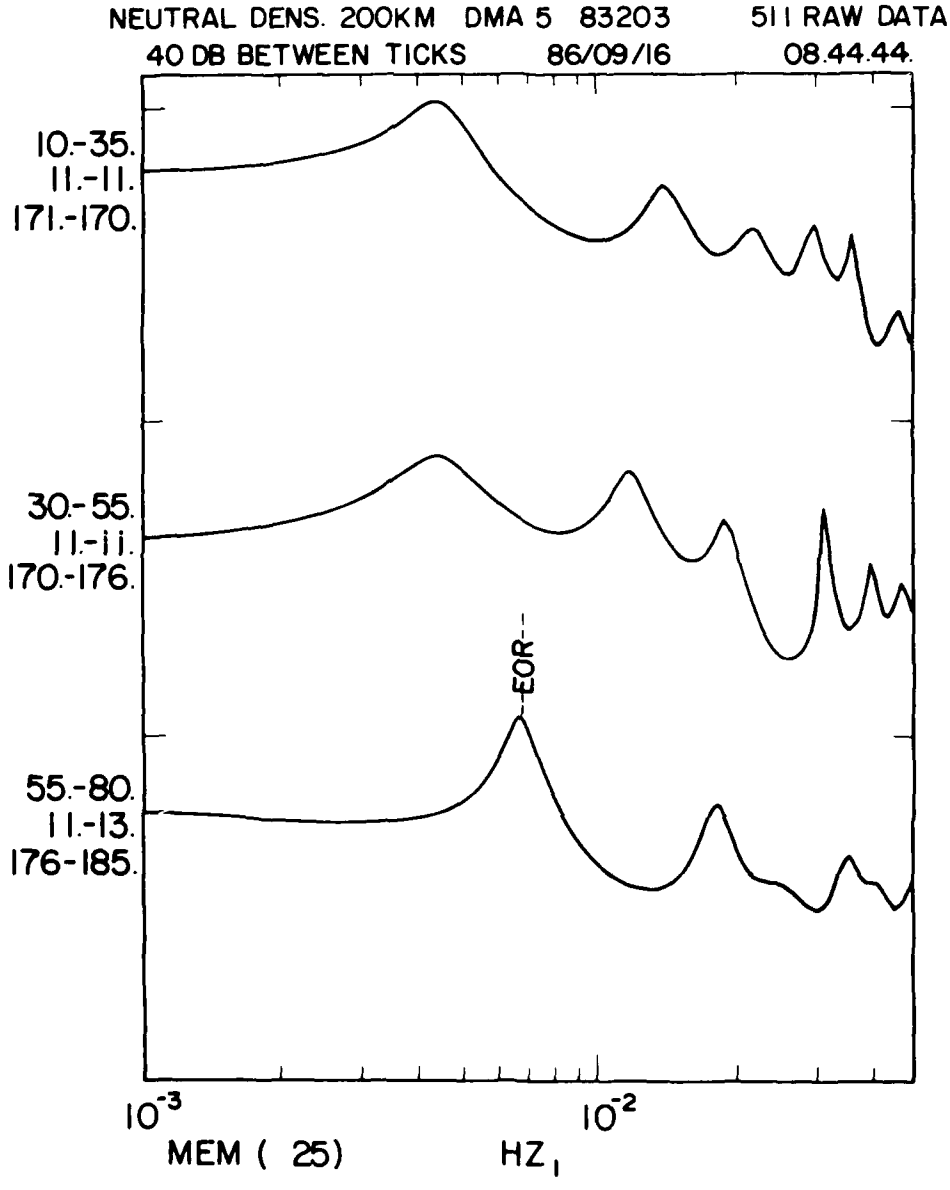

Figure 9. MEM Spectra (power spectral density vs frequency) of Order = 25 for Daytime (~ 1030 h) Portion of Rev 511. Tick marks correspond to 40-dB points for power spectral density

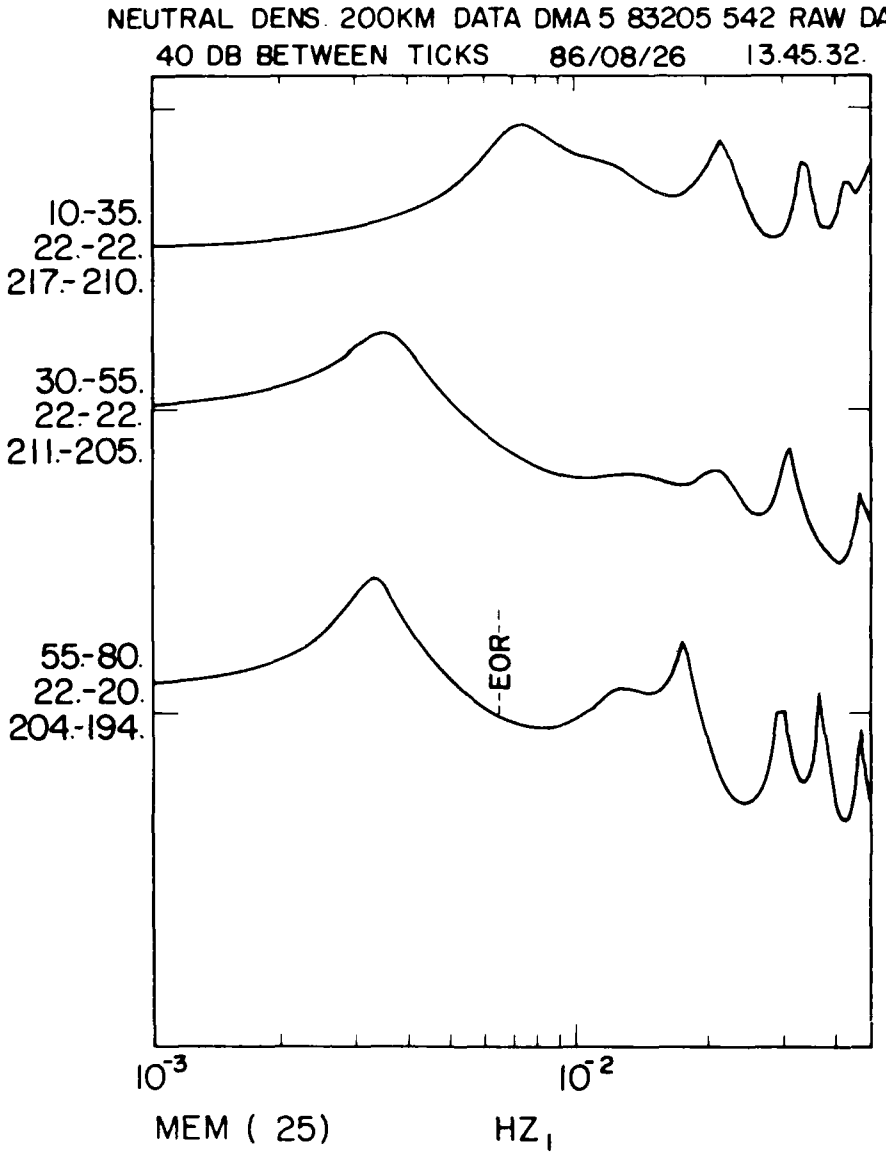

Figure 10. MEM Spectra (power spectral density vs frequency) of Order = 25 for Nightside (~ 2030 h) Portion of Rev. 542. Tick marks correspond to 40-dB points for power spectral density

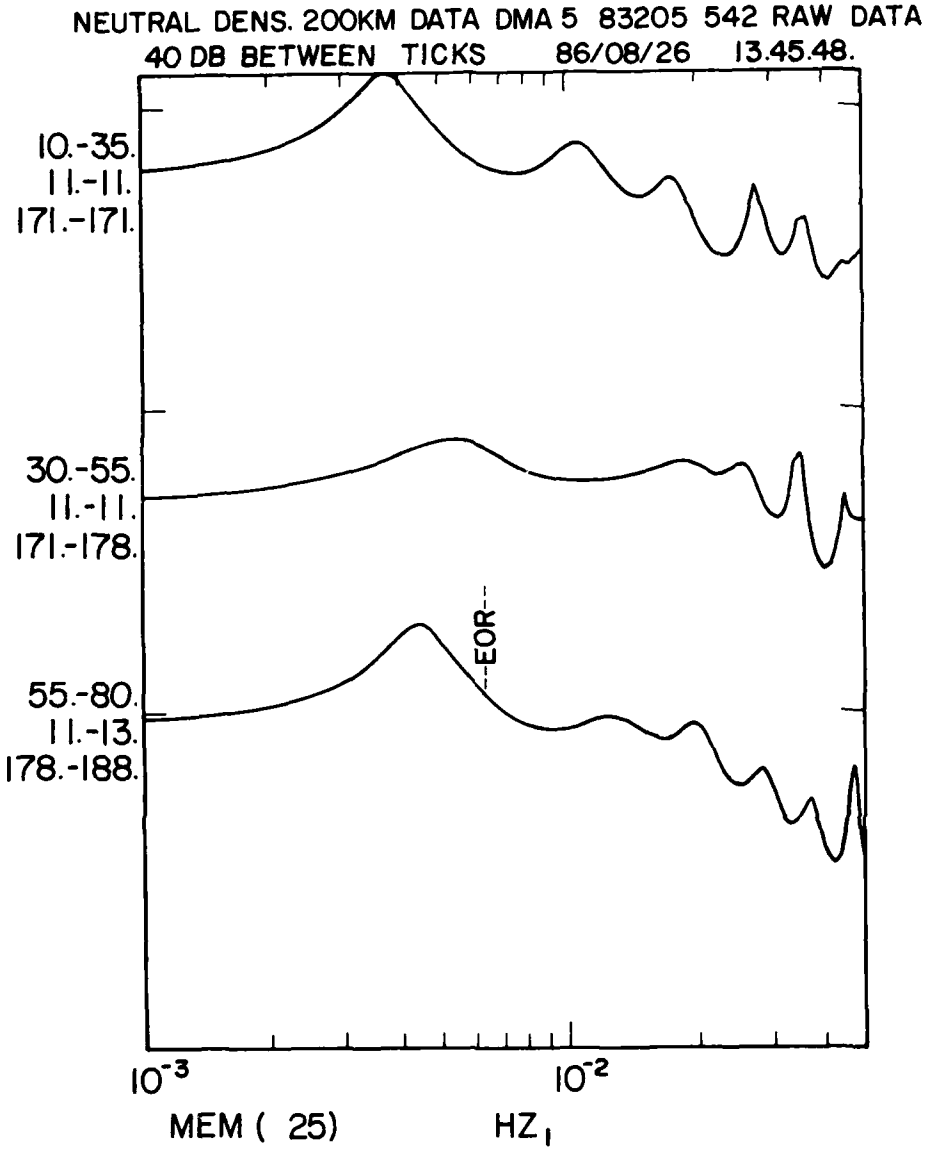

Figure 11. MEM Spectra (power spectral density vs frequency) of Order = 25 for Daytime (~ 1030 h) Portion of Rev 542. Tick marks correspond to 40-dB points for power spectral density

Table 1. Percent Occurrence of ≧ 30 dB Spectral Peaks as a Function of Horizontal Wavelength

		Horizontal Wavelength (km)				
		"Large-Scale"			"Medium Scale"	
Latitude	Local Time	1250-2500	750-1250	500-750	250-500	150-250
(DAY 203)						
10° - 35°	2030	46	31	23	69	54
30° - 55°	2030	62	23	31	46	23
55° - 80°	2030	79	14	43	71	29
10° - 35°	1030	92	15	39	15	15
30° - 55°	1030	64	36	36	36	9
55° - 80°	1030	77	15	62	23	0
(DAY 205)						
10° - 35°	2030	67	17	42	67	92
30° - 55°	2030	77	23	46	85	85
55° - 80°	2030	92	8	62	77	77
10° - 35°	1030	62	23	38	54	38
30° - 55°	1030	83	33	42	92	42
55° - 80°	1030	100	18	27	73	36
(Differences, DAY 205-203)						
10° - 35°	2030	+21	-14	+19	-2	+38
30° - 55°	2030	+15	0	+15	+39	+62
55° - 80°	2030	+13	-6	+19	+6	+48
10° - 35°	1030	-30	+8	-1	+49	+23
30° - 55°	1030	+19	-3	+6	+56	+33
55° - 80°	1030	+23	+3	-35	+50	+36

Table 2. Percent Occurrence of ≧ 40 dB Spectral Peaks as a Function of Horizontal Wavelength

		Horizontal Wavelength (km)				
		"Large Scale"			"Medium Scale"	
Latitude	Local Time	1250-2500	750-1250	500-750	250-500	150-125
(DAY 203)						
10° - 35°	2030	15	0	0	0	0
30° - 55°	2030	31	8	0	0	0
55° - 80°	2030	46	0	15	8	8
10° - 35°	1030	38	0	0	0	0
30° - 55°	1030	8	0	0	0	0
55° - 80°	1030	15	15	0	0	0
(DAY 205)						
10° - 35°	2030	25	0	8	0	8
30° - 55°	2030	46	15	0	8	0
55° - 80°	2030	69	8	23	15	15
10° - 35°	1030	23	8	0	0	0
30° - 55°	1030	38	8	0	0	0
55° - 80°	1030	54	0	8	0	0

4. CONCLUSIONS

Density data from the Satellite Electrostatic Triaxial Accelerometer (SETA) experiment were spectrally analyzed by the Maximum Entropy Method (MEM). Spectra were computed for typical magnetically quiet and active days during July 1983, and the relative occurrence of spectral peaks in wavelength ranges of large-scale (hundreds to thousands of kilometers) TIDs is examined as a function of local time and latitude. We preliminarily conclude from analysis of these data the following:

(a) Wave motions contribute to the observed variability of density during both quiet and active conditions, and become increasingly important as magnetic disturbances become more intense.

(b) There exists evidence for enhanced wave activity at high latitudes and during nighttime.

(c) There exists a significantly higher probability of finding waves of horizontal wavelengths between 1250 to 2000 km and 150 to 500 km, especially during geomagnetically disturbed conditions, as opposed to those waves with wavelengths between 500 and 1250 km. The former, larger-scale waves, are known to be capable of propagating large distances with little attenuation. We tentatively conclude that the relatively frequent occurrence of the shorter-scale waves, even at low latitudes, may be attributable to ducting in the lower thermosphere which allows them to travel large distances as suggested by Mayr et al. [1,2]

These preliminary findings can be verified and further refined through analysis of additional satellite density data now in existence. The present report provides a computerized procedure to process these data to reveal the dominant wave characteristics, and a rationale and direction to future scientific efforts along these lines.

References

1. Mayr, H.G., Harris, I., Varosi, F., and Herrero, F.A. (1984) Global excitation of wave phenomena in a dissipative multiconstituent medium. 1. Transfer function of the Earth's thermosphere, J. Geophys. Res., 89:10929.
2. Mayr, H.G., Harris, I., Varosi, F., and Herrero, F.A. (1984) Global excitation of wave phenomena in a dissipative multiconstituent medium. 2. Impulsive perturbations in the Earth's thermosphere, J. Geophys. Res., 89:10961.
3. Georges, T.M. (1968) HF Doppler studies of travelling ionospheric disturbances, J. Atmos. Terr. Phys., 30:735.
4. Testud, J. (1970) Gravity waves generated during magnetic substorms, J. Atmos. Terr. Phys., 32:1793.
5. Thome, G. (1968) Long-period waves generated in the polar ionosphere during the onset of magnetic storms, J. Geophys. Res., 73:6319.
6. Davis, M.J., and da Rosa, A.V. (1969) Traveling ionospheric disturbances originating in the auroral oval during polar substorms, J. Geophys. Res., 74:5721.
7. Testud, J.P., Amayenc, P., and Blanc, M. (1975) Middle and low latitude effects of auroral disturbances from incoherent scatter, J. Atmos. Terr. Phys., 37:989.
8. Harper, R.M. (1972) Observation of a large nighttime gravity wave at Arecibo, J. Geophys. Res., 77:1311.
9. Herrero, F.A., and Meriwether, J.W. (1981) Equatorial nighttime F-region events: A survey of 6300 Å airglow intensity maps at Arecibo, J. Atmos. Terr. Phys., 43:859.
10. Beer, T. (1974) Atmospheric Waves. John Wiley, New York.
11. Larsen, M.F., Swartz, W.E., and Woodman, R.F. (1982) Gravity wave generation by thunderstorms observed with a vertically-pointing 430 MHz radar, Geophys. Res. Lett., 9:571.

References

12. Mastrantonio, G.F., Einaudi, F., Fua, D., and Lalas, D.P. (1976) Generation of gravity waves by jet streams in the atmosphere, J. Atmos. Sci., 33:1730.

13. Bertin, F.J., Testud, J., Kersley, L., and Rees, P.R. (1978) The meteorological jet stream as a source of medium scale gravity waves in the thermosphere: An experimental study, J. Atmos. Terr. Phys., 40:1161.

14. Richmond, A.D. (1978) The nature of gravity wave ducting in the thermosphere, J. Geophys. Res., 83:1385.

15. Francis, S.H. (1974) A theory of medium-scale traveling ionospheric disturbances, J. Geophys. Res., 79:5245.

16. Hines, C.O. (1960) Internal atmospheric gravity waves at ionospheric heights, Can. J. Phys., 38:1441.

17. Friedman, J.P. (1966) Propagation of internal gravity waves in a thermally stratified atmosphere, J. Geophys. Res., 71:1033.

18. Gross, S.H., Reber, C.A., and Huang, F.T. (1984) Large-scale waves in the thermosphere observed by the AE-C satellite, IEEE Trans. on Geos. and Remote Sens., GE-22:340.

19. Marcos, F.A. (1987) Requirements for improved thermospheric models, J. Astronaut. Sci., in press.

20. Champion, K.S.W., and Marcos, F.A. (1973) The triaxial accelerometer system on Atmosphere Explorer, Radio Sci., 8:197.

21. Marcos, F.A., and Swift, E.R. (1982) Application of the Satellite Triaxial Accelerometer Experiment to Atmospheric Density and Wind Studies, AFGL-TR-82-0091, AD A120852.

22. Noonan, J.P., Fioretti, R.W., and Hass, B. (1975) Digital Filtering Analysis Applied to the Atmosphere Explorer-C Satellite MESA Accelerometer Data, AFCRL-TR-75-0293, AD A015765.

23. Jacchia, L.G. (1971) Revised Static Models of the Thermosphere and Exosphere With Empirical Temperature Profiles, Spec. Rept. 332, Smithsonian Astrophys. Observatory, Cambridge, Massachusetts.

24. Sentman, L.H. (1961) Free molecular flow theory and its application to the determination of aerodynamic forces, Rept. LMSC-448514, Lockheed Missiles and Space Co., Sunnyvale, California.

25. Radoski, H.R., Fougere, P.F., and Zawalick, E.J. (1975) A comparison of power spectral estimates and applications of the maximum entropy method, J. Geophys. Res., 80:619.

26. Burg, J.P. (1981) Maximum entropy spectral analysis in Modern Spectrum Analysis, edited by D.G. Childers. IEEE Press, New York

27. Ulrych, T.J., and Bishop, T.N. (1975) Maximum entropy spectral analysis and autoregressive decomposition, Rev. Geophys. Space Phys., 13:183.

28. Roble, R.G., Forbes, J.M., and Marcos, F.A. (1987) Thermospheric dynamics during the March 22, 1979 magnetic storm (1.) Model simulations, J. Geophys. Res., 92:6045.

29. Forbes, J.M., Roble, R.G., and Marcos, F.A. (1987) Thermospheric dynamics during the March 22, 1979 magnetic storm (2.) Comparisons of model predictions with observations, J. Geophys. Res., 92:6069.

END

DATE

FILMED

8-88

DTIC